Original Article

JCBFM

Journal of Cerebral Blood Flow & Metabolism
2017, Vol. 37(6) 2149–2158

DOI: 10.1177/0271678X16661340
journals.sagepub.com/home/jcbfm
SAGE

Changes in intracranial venous blood flow and pulsatility in Alzheimer's disease: A 4D flow MRI study

Leonardo A Rivera-Rivera[1,*], Tilman Schubert[2,3,*], Patrick Turski[1,2], Kevin M Johnson[1], Sara E Berman[4], Howard A Rowley[2], Cynthia M Carlsson[4,5,6], Sterling C Johnson[4,5,6] and Oliver Wieben[1,2]

Abstract

Cerebral blood flow, arterial pulsation, and vasomotion may be important indicators of cerebrovascular health in aging and diseases of aging such as Alzheimer's disease. Noninvasive markers that assess these characteristics may be helpful in the study of co-occurrence of these diseases and potential additive and interacting effects. In this study, 4D flow MRI was used to measure intra-cranial flow features with cardiac-gated phase contrast MRI in cranial arteries and veins. Mean blood flow and pulsatility index as well as the transit time of the peak flow from the middle cerebral artery to the superior sagittal sinus were measured in a total of 104 subjects comprising of four groups: (a) subjects with Alzheimer's disease, (b) age-matched controls, (c) subjects with mild cognitive impairment, and (d) a group of late middle-aged with parental history of sporadic Alzheimer's disease. The Alzheimer's disease group exhibited: a significant decrease in mean blood flow in the superior sagittal sinus, transverse sinus, middle cerebral artery, and internal carotid arteries; a significant decrease of the peak and end diastolic blood flow in the middle cerebral artery and superior sagittal sinus; a faster transmission of peak flow from the middle cerebral artery to the superior sagittal sinus and increased pulsatility index along the carotid siphon.

Keywords

Alzheimer's disease, mild cognitive impairment, 4D flow MRI, mean blood flow, pulsatility index

Received 4 April 2016; Revised 16 June 2016; Accepted 23 June 2016

Introduction

Sporadic late onset Alzheimer's disease (AD) is the most common cause of dementia in the elderly population.[1] The dementia syndrome of AD is clinically diagnosed by a history of slowly progressive loss of cognitive function in two or more cognitive domains that impairs day to day functioning.[1] Classic neuropathological findings on post-mortem brain specimens consist of increased extracellular beta amyloid (Aβ) deposits and the presence of neurofibrillary tangles within affected neurons.[2] Therefore, AD was for a long time regarded as a distinctive, non-vascular type of dementia.[3]

However, evidence is increasing that pathologic alterations of the vasculature may play a role in AD dementia. Initially only thought to be the underlying cause for dementia related to stroke or leukoencephalopathy,

[1]Department of Medical Physics, University of Wisconsin School of Medicine and Public Health, Madison, USA
[2]Department of Radiology, University of Wisconsin School of Medicine and Public Health, Madison, USA
[3]Clinic of Radiology and Nuclear Medicine, Basel University Hospital, Basel, Switzerland
[4]Alzheimer's Disease Research Center, University of Wisconsin School of Medicine and Public Health, Madison, USA
[5]Geriatric Research Education and Clinical Center, Wm. S. Middleton Memorial VA Hospital, Madison, USA
[6]Wisconsin Alzheimer's Institute, University of Wisconsin School of Medicine and Public Health, Madison, USA
*These authors contributed equally to this work.

Corresponding author:
Oliver Wieben, University of Wisconsin-Madison, Rm 1127, Wisconsin Institute for Medical Research, 1111 Highland Ave, Madison, WI 53705-2275, USA.
Email: owieben@wisc.edu

it has been observed that altered and dysfunctional cerebral vasculature is also present in classical clinically diagnosed AD type dementia.[4–9]

To date, disagreement persists if alterations of the cerebrovasculature are a contributing cause or result of the neurodegenerative changes typically observed in AD, or if vascular and neuronal changes appear simultaneously throughout the course of the disease.[3,10,11] One proposed mechanism by which pathologic changes of the cerebrovasculature might affect the evolution of the disease is an increase in pulsatility due to reduced vascular compliance, as has been reported in AD patients.[12,13] The brain may be especially vulnerable to increased arterial pulsatility due to the low resistive abilities of the brain arterioles. The constant, high demand of blood makes it impossible to employ strong precapillary sphincters that would protect the brain from increased pulsatility.[14–16] This characteristic of the brain is underlined by the finding that the large conducting arteries seem to have specific properties to decrease arterial pulsatility to the brain along their course.[17–19]

It has been suggested in recent work that reduction in vascular elasticity and expansive and contractile forces change the amplitude and length of the arterial pulse and may affect the perivascular clearance of interstitial fluid, diminishing the physiologic transport of metabolites out of the brain including beta-amyloid (Aβ).[8,20–24]

Consequently, there is interest in non-invasive methods to assess cerebrovascular hemodynamics as potential systemic pathogenic or exacerbating factors in AD and potential avenues for treatment.[25]

Transcranial Doppler (TCD) ultrasound and 2D phase contrast (PC) MRI are two distinct common approaches used to probe intracranial hemodynamic parameters. TCD, however, has a limited ability to detect distal branches of intracranial vessels and does not assess vessel diameter while 2D PC MRI is time consuming since each vessel segment requires the acquisition of an additional cardiac gated flow sensitive acquisition prescribed orthogonal to the local vessel orientation. With these limitations, neither technique is well suited for a comprehensive and reproducible intracranial hemodynamic analysis.

Recent advances in MR hardware, data acquisition, and reconstruction methodology have facilitated the use of 4D flow MRI in clinically feasible scan times. This approach enables both volumetric angiographic and quantitative assessment of blood flow velocities in a single acquisition.[26] The velocity flow field is captured at multiple phases of the cardiac cycle in a volumetric acquisition with three-directional velocity encoding. With adequate spatial and temporal resolution, such 4D flow MRI approaches are well-suited for comprehensive cranial hemodynamic assessment. The complete cerebral vasculature is included in the imaging volume and any vessel can be evaluated for geometry and hemodynamic parameters after scan completion.

One particularly well suited approach for the high resolution demands of intracranial 4D flow MRI is PC VIPR (Phase Contrast Vastly undersampled Isotropic Projection), which utilizes radial undersampling for accelerated acquisitions with small voxel sizes.[27] This technique has been validated in various vascular territories, including the renal arteries, thorax, and cranial vasculature.[28–30]

Recently, it was shown that mean blood flow decreases and PI increases with age and AD symptoms in the major cerebral arteries.[9] However, less information is available regarding changes in the venous system and the translation of pulsatile flow from arteries to veins in AD and mild cognitive impaired compared with healthy individuals.

Therefore, the purpose of this work was an integrated assessment of the cerebral vasculature. In this study, we used PC VIPR to quantify blood flow patterns in the proximal middle cerebral artery (MCA) and internal carotid artery (ICA) as well as the sagittal, straight, and transverse sinus in four different patient cohorts: (a) patients with dementia due to AD, (b) mild cognitive impairment, and (c) age-matched controls as well as a fourth group consisting of late middle-aged healthy adults with a parental history of late onset sporadic AD.

Materials and methods

Subjects and clinical classification

A total of 104 participants from the Wisconsin Alzheimer's Disease Research Center Clinical Core underwent comprehensive MRI brain imaging as part of studies on memory, aging, and risk for AD. Of these recruited individuals, 26 were cognitively normal older controls (age range = 66–85 years, mean = 73 years, 12 F), 26 AD patients (age range = 57–89 years, mean = 71 years, 11 F) and 26 mild cognitive impairment (MCI) patients (age range = 52–86 years, mean = 73 years, 13 F). A cognitively healthy middle-aged group with parental history of sporadic Alzheimer's disease (MAPHSA) included 26 adults (age range = 45–64 years, mean = 57 years, 22 F).[31] The MAPHSA group is enriched for risk factors that predispose to AD, but they are not a pre-MCI group. All of these individuals were diagnostically characterized as described in previous work.[9,32] The present study consists of 85 subjects that had been included in a prior manuscript and 19 new subjects.[9] The analysis was expanded beyond the prior study by introducing measures of venous flow and pulse wave transit time. All data (arterial and venous) have been reprocessed with an improved flow data analysis tool that is based on automated vessel segmentation and analysis that has shown to be

less user dependent and thereby more reproducible especially when using larger sets of data. The University of Wisconsin Institutional Review Board approved all study procedures and protocols following the policies and guidance established by the campus Human Research Protection Program (HRPP) and each participant provided signed informed consent before participation.

Cognitive assessment

The population of the present study is part of the large National Alzheimer's Coordinating Center's (NACC) Uniform Dataset. Data collection was performed as described in previous work.[9] Subjects given a consensus diagnosis of a non-Alzheimer's variant of dementia, such as Frontotemporal Dementia, Lewy Body Dementia, or Vascular Dementia, were excluded from this study.

MR imaging protocol

Participants were scanned using a 3T clinical MRI system (MR750, GE Healthcare, Waukesha, WI) with an eight-channel head coil (Excite HD Brain Coil, GE Healthcare, Waukesha, WI). Volumetric, cardiac time-resolved PC MRI data with three-directional velocity encoding were acquired with a 3D radially undersampled sequence (PC VIPR), with the following imaging parameters: velocity encoding (venc) = 80 cm/s, imaging volume = $(22 \times 22 \times 16\,cm^3)$, acquired isotropic spatial resolution = $(0.7\,mm)^3$, repetition time (TR)/echo time (TE) = 7.4/2.7 ms, 14,000 projection angles, scan time ~ 7 min, flip angle $\alpha = 10^\circ$, bandwidth = 83.3 kHz.[33,34] Time averaged magnitude and velocity data were generated via an offline reconstruction for all subjects. For each subject, cardiac triggers were collected from a photoplethysmogram on a pulse oxymeter worn on the subject's finger during the exam. Utilizing this trigger data, cardiac cycle resolved data were retrospectively reconstructed utilizing 20 cardiac phases with a spatially adaptive temporal interpolation.[35] Figure 1 shows an example of PC VIPR data as (a) sagittal, (b) coronal, and (c) axial maximum intensity projection (MIP) images of the PC angiogram, derived by combining the magnitude and the mean velocity data.

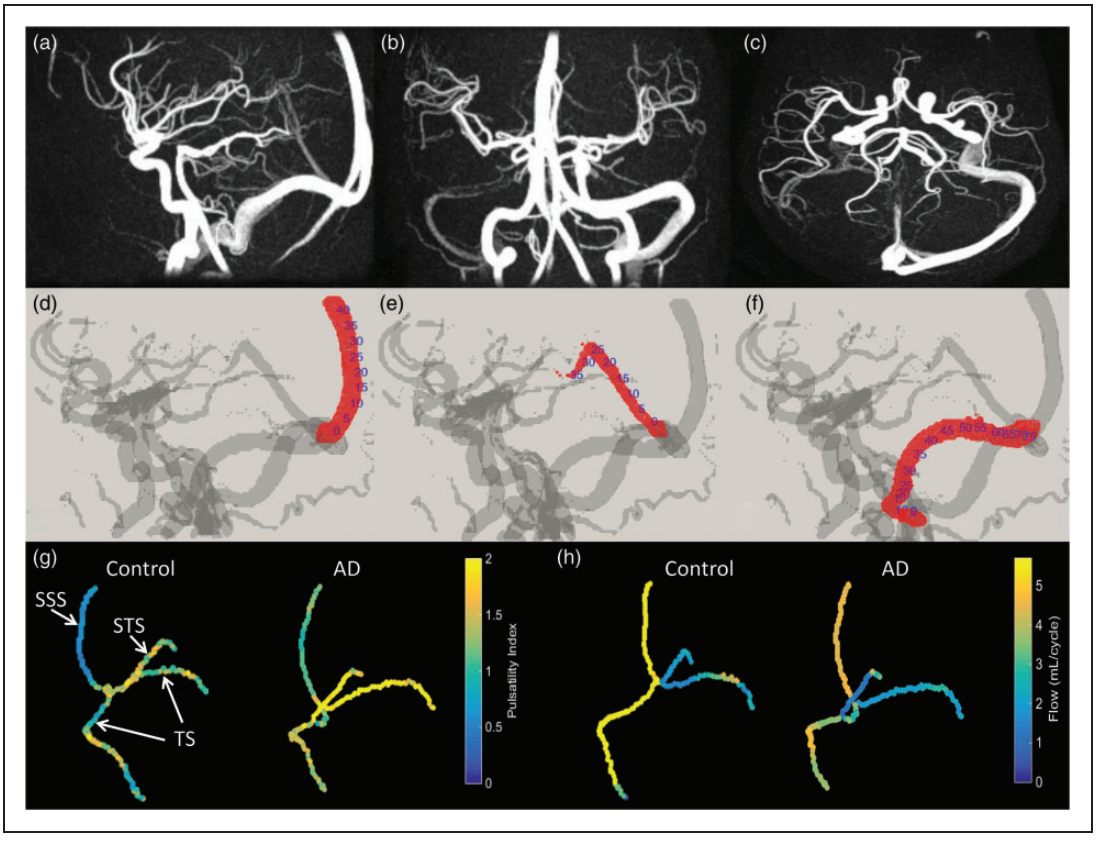

Figure 1. PC VIPR data shown as (a) sagittal, (b) coronal, (c) axial MIP image of the PC angiogram and the segmented 3D vessels with centerline points labels for the (d) superior sagittal sinus (SSS), (e) straight sinus (STS), and (f) transverse sinus (TS) extracted from the PC VIPR data. (g) Pulsatility index and (h) mean blood flow (mL/s) throughout the major venous segments shown as color maps for one age-matched control and one AD subject.

Processing: Flow analysis

Automatic vessel segmentation and flow quantification were performed in a customized post-processing tool (MATLAB, Mathworks, Natick, MA).[36] Time maximum intensity projection (tMIP) images were reconstructed from dynamic PC MR angiograms derived from the 4D flow data. The vascular tree was extracted using a centerline process, recording coordinates, and labels for every branch. A centerline guided flow tracking algorithm was used to visualize and select the vessel segments for further analysis. Flow rates were calculated for every selected branch by averaging flow data obtained in local cross-sectional cut-planes automatically placed in every centerline point perpendicular to the axial direction of the vessel. For this purpose, four venous segments were selected (Figure 1(d) to (f)): posteroinferior portion of the SSS, middle segment of the straight sinus (STS), and the transverse sinus (TS) (left and right) segment just before the sigmoid sinus. Additionally, four arterial segments were included: distal cervical ICA (left and right) and MCA (left and right). Mean blood flow (MBF) and pulsatility index (PI = (Qmax − Qmin)/Qmean; Q = flow) were calculated for all vessel segments and groups. The pulsatile flow waveform as a function of the cardiac cycle was used to compute MBF and PI, as well to calculate the peak flow, end diastolic flow, and transit time of the waveform peak between the MCA and SSS. The pulsatility along the carotid siphon was investigated by computing the PI ratio from the MCA to ICA.

Statistical analysis

Values for mean blood flow, and PI across the vessel segments were compared between all four populations (AD, MCI, age-matched controls, and MAPHSA). The final count of vessel segments was 208 ICAs, 208 MCAs, 104 SSS, 83 STS, and 208 TS. Twenty-one STS vessel segments could not be analyzed because the velocities were so slow that their signal was undetectable since the venc of 80 cm/s was optimized for the highest anticipated velocities in the arterial system. The association between group and vessel segment was assessed using ANOVA followed by Tukey's Honestly Significant Difference Procedure for pairwise comparison for adjusted means. Statistical analysis was conducted in MATLAB (The Mathworks, Natick, MA).

Results

Hemodynamic parameters

Results for the hemodynamic analysis are summarized for all vessel segments in Figures 2–6. Statistically

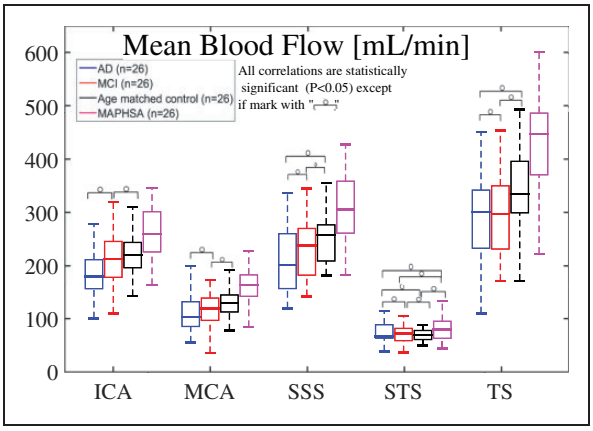

Figure 2. Mean blood flow (mL/min) for 104 subjects including AD (n = 26), MCI (n = 26), age-matched controls (n = 26), and MAPHSA (n = 26). The four populations were compared with each vessel segment using ANOVA followed by Tukey's Honestly Significant Difference Procedure.

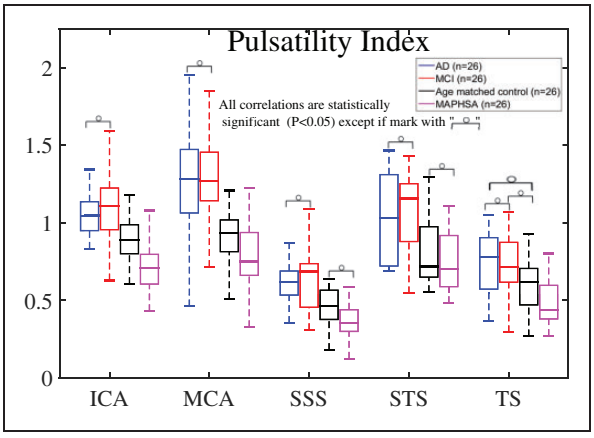

Figure 3. Pulsatility Index for 104 subjects including AD (n = 26), MCI (n = 26), age-matched controls (n = 26), and MAPHSA (n = 26).

significant differences were found for the PI (Figure 3) between the AD, MCI, age-matched controls, and the MAPHSA group in the ICA, MCA, SSS, STS, and TS. This was also true for mean blood flow except for the STS segment where no significant differences were found. The box plots contain the median values and standard deviation for the analyzed parameters. In addition, pairs that were found not to be statistically different are marked in the figures. Significant differences were found in the MCA/ICA PI ratio (Figure 4). The transit time of the peak flow from MCA to SSS was significantly different between the AD group and age-matched controls and between the MAPHSA and age-matched controls. Peak and minimum blood flow in the MCA and the SSS was significantly different between the AD group and age-matched controls

(Table 1). No statistically significant differences were found in systolic and diastolic blood pressure measurements between the three age-matched groups (AD, MCI, and age-matched controls; Supplementary Material). ROC analysis, demographics, and health characteristics of the subjects are available as supplementary material.

AD group

Pulsatility index. The AD group exhibited a significant higher pulsatility index in all vessel segments when compared with the MAPHSA group. When compared with the age-matched controls, the AD group exhibited a significant higher PI for all vessel segments except the TS segment. No significant difference was found between the PI of the AD and MCI groups. The MCA/ICA PI ratio was statistically higher in the AD group when compared with the age-matched controls ($P < 0.001$) and was the highest among all the groups.

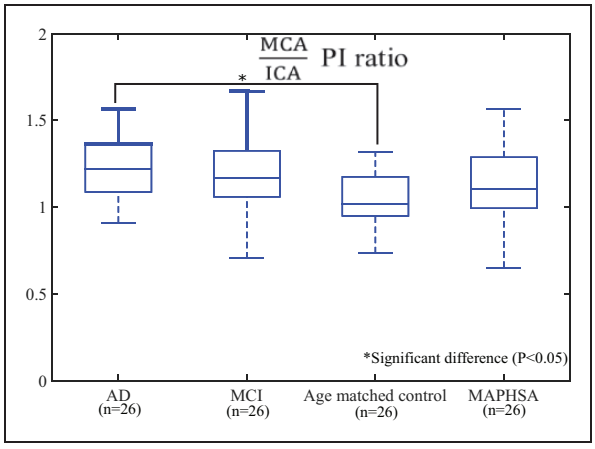

Figure 4. MCA/ICA PI ratios for 104 subjects including patients with AD, MCI, age-matched controls, and a MAPHSA group. Statistically significant differences were found between AD and age-matched controls and are indicated with a "*" (*$P < 0.001$).

Mean blood flow. The AD group exhibited a statistically significant decrease of MBF in all the vessel segments when compared with the MAPHSA group, except on the STS segment. When compared with the age-matched control group, the AD group had a statistically significant decrease of MBF in the cervical ICA and MCA segments; no significant difference was found in the SSS, STS, and TS segments. The AD group reported a lower MBF for most segments went compared with the MCI group, but no significant differences were found.

Pulsatile cardiac waveform. The cardiac waveform of the pulsatile flow in the MCA and SSS are shown in Figures 5 and 6. The AD group exhibited the smallest amplitude in the pulsatile flow when compared with the other three groups. The AD group time to peak flow in the MCA and SSS were 385 ms and 484 ms, respectively, with a 99 ms transit time between the peaks. The AD group exhibited the shortest transit time of the peak flow from the MCA to the SSS when compared with the other three groups. The AD group transit time of the peak flow from MCA to SSS was significantly shorter than in the age-matched controls. The peak flow in the MCA and SSS was the lowest for the AD group among the four groups, reaching

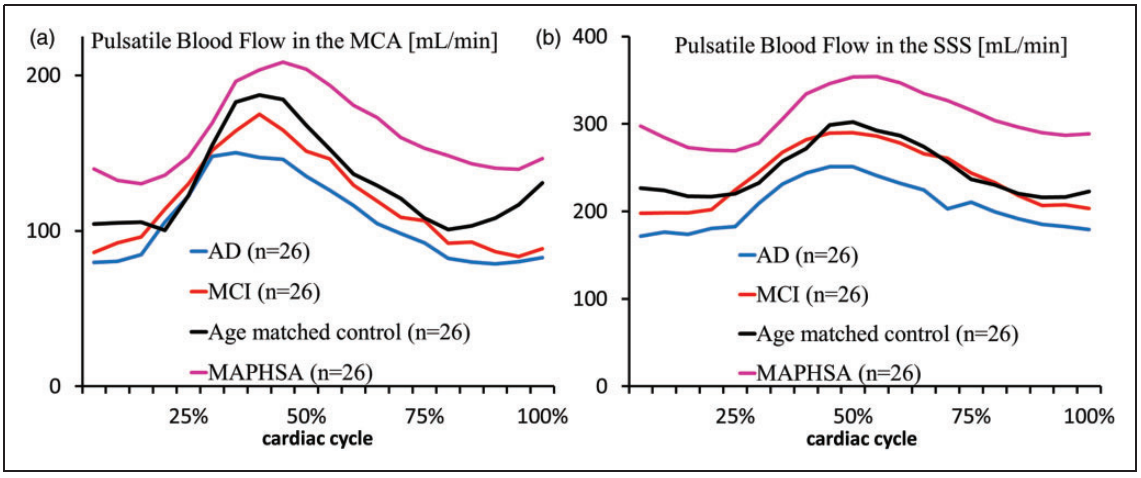

Figure 5. Pulsatile flow (mL/min) through the cardiac cycle (%) in the MCA (a) and SSS (b) for 104 subjects including patients with AD, MCI, age-matched controls, and a MAPHSA group. Each curve represents the average pulsatile flow per each group.

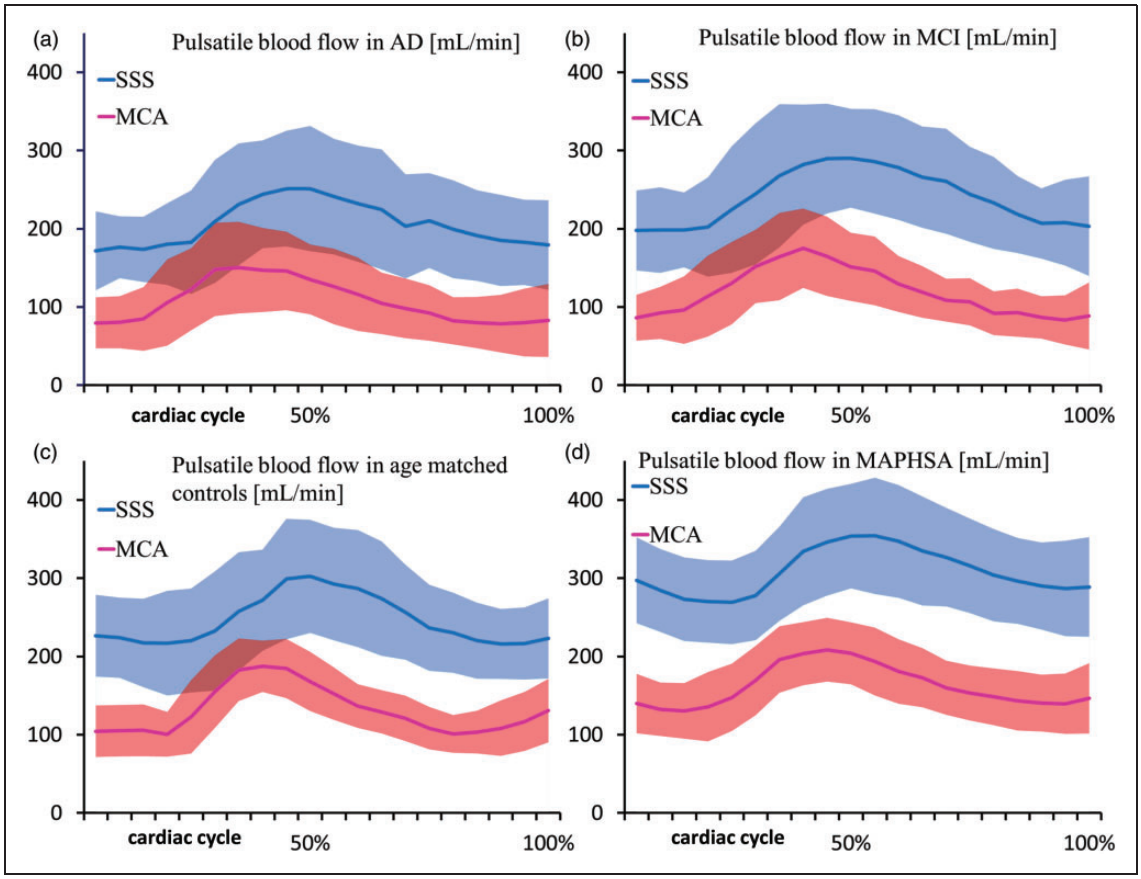

Figure 6. Superimposed pulsatile flow (mL/min) through the cardiac cycle (%) in the MCA and SSS for 104 subjects including patients with AD (a), MCI (b), age-matched controls (c), and a MAPHSA group (d). The solid lines represent the average pulsatile flow per group, while the shades describe the standard deviations.

Table 1. Transit time of the peak blood flow from the MCA to SSS and range of the flow rates.

	AD (n = 26)	MCI (n = 26)	Age-matched control (n = 26)	MAPHSA (n = 26)
Time (ms)				
Time to peak in MCA	385 ± 85	357 ± 71	349 ± 93	402 ± 91
Time to peak in SSS	484 ± 91	465 ± 83	520 ± 99	508 ± 97
Time to peak (SSS-MCA)	99 ± 93	108 ± 57	171 ± 77	106 ± 91
Flow (mL/min)				
Peak flow MCA	183 ± 60	207 ± 43	212 ± 36	230 ± 42
Minimum flow MCA	53 ± 26	62 ± 20	84 ± 23	116 ± 26
Peak flow SSS	281 ± 82	317 ± 79	319 ± 86	370 ± 77
Minimum flow SSS	141 ± 43	168 ± 44	195 ± 43	256 ± 48

MCI: mild cognitive impairment; MCA: middle cerebral artery; SSS: superior sagittal sinus.

significant differences with the MAPHSA group. The minimum flow in the MCA and SSS were the lowest for the AD population and these differences were statistically significant when compared with the age-matched controls and the MAPHSA group.

MCI group

Pulsatility index. The MCI group exhibited a statistically significant higher pulsatility index in all vessel segments when compared with the MAPHSA group.

When compared with the age-matched controls, the MCI group exhibited a significantly higher PI for all vessel segments except in the TS segment. The MCA/ICA PI ratio was higher in the MCI group when compared with the age-matched controls but not statistically different. The mean value of the MCA/ICA PI ratio was the same for the MCI and MAPHSA groups.

Mean blood flow. The MCI group exhibited a statistically significant decrease of MBF in all the vessel segments when compared with the MAPHSA group, except on the STS segment. No significant differences in MBF were found between the MCI and age-matched controls.

Pulsatile cardiac waveform. The MCI group time to peak flow in the MCA and SSS were 357 ms and 465 ms, respectively, with a 108 ms difference between the peaks. The MCI group mean transit time of the peak flow was significantly shorter than in the age-matched controls, but similar to the MAPHSA group. The peak blood flow in the MCA and the SSS was lower in the MCI group when compared with the age-matched control and the MAPHSA groups. The minimum blood flow in the MCA was statistically lower in the MCI group when compared with the age-matched control and MAPHSA groups. In the SSS, the minimum blood flow was significantly lower in the MCI group when compared with the MAPHSA group.

Age-matched control group and MAPHSA

Pulsatility index. The age-matched control group exhibited a higher pulsatility index in all vessel segments when compared with the MAPHSA group, with differences in the MCA, ICA, and TS that reached statistical significance. Interestingly, the MCA/ICA PI ratio was smaller in the age-matched controls than in the MAPHSA group, but not significantly different.

Mean blood flow. The age-matched control group had a statistically significant decrease in MBF in all vessel segments analyzed when compared with the MAPHSA group, except on the STS segment.

Pulsatile cardiac waveform. Time to peak flow in the MCA and SSS were 385 ms and 484 ms, respectively, for the age-matched control group, with a 171 ms difference between the peaks. The age-matched control group exhibited the longest transit time of the peak flow from the MCA to the SSS when compared with the other three groups. The MAPHSA group time to peak flow in the MCA and SSS were 402 ms and 508 ms, respectively, with a 106 ms difference between the peaks. This mean transit time is significantly shorter than in the (older) age-matched controls. The peak blood flow in the MCA and SSS was lower in the age-matched control group when compared with the MAPHSA group. The minimum blood flow was significantly lower in the age-matched controls when compared with the MAPHSA group.

Discussion

In this study, we investigated and compared cerebral blood flow patterns in a large cohort of individuals including AD and MCI patients, healthy age-matched controls and younger individuals with parental history of AD. In all arterial and venous locations, we observed a significantly increased Pulsatility Index in patients with AD and MCI compared with age-matched controls and individuals with parental history of sporadic AD. The PI ratio MCA/ICA was significantly higher in AD patients compared with age-matched controls ($P < 0.001$). Furthermore, total mean arterial blood flow was significantly lower in subjects with AD compared with the other groups. The time delay from the arterial peak in the MCA to the venous peak in the SSS was significantly longer in healthy age-matched controls than in patients with AD, MCI, and, unexpectedly, longer than in the MAPHSA group.

Our results of increased PI in AD and MCI patients compared with age-matched controls are in accordance with other studies.[15] With aging, stiffening of the vessel wall leads to reduced dampening of the pressure pulse wave while traveling through the arterial tree. Thus, in old compared with young individuals, the peak amplitude of the pressure and resulting flow wave will be better maintained as the pulse propagates down the vascular tree.[37] To follow the Monroe-Kellie doctrine stating that an increase of one fluid in a rigid container must displace another, the arterial pulse wave drives cerebrospinal fluid (CSF) and venous blood out of the cranial cavity. CSF flow in and out of the cranial cavity therefore helps to reduce the net brain volume change. Increased arterial pulsatility can be compensated by increased CSF pulsations up to a certain degree.[38] This compensation is reflected by a lower venous pulsatility in healthy age-matched controls compared with AD and MCI patients in our study. In AD and MCI patients, however, CSF pulse volume does not sufficiently compensate for the further increased arterial pulsatility and venous blood must be pushed out of the cranial cavity accordingly. This is reflected by a higher venous PI in the superior sagittal sinus, straight sinus, and transverse sinus in AD and MCI compared with age-matched controls and MAPHSA individuals. An increase in cerebral venous pulsatility has been reported to associate with aging

and, more pronounced, in senile dementia.[13,39,40] These changes could also indicate an increased vascular resistance on the capillary bed, thereby reducing the total compliance and subsequently increasing the Pulsatility Index in the whole system.

The reduced mean blood flow in the SSS but similar values in the ST in AD patients when compared with age-matched controls might reflect a relative decrease in cortical cerebral blood volume. However, recruitment of alternative cortical drainage networks may also play a role in this observation.

The significantly faster translation of the peak of the flow waveform from the MCA to the SSS in the AD and MCI groups when compared with the age-matched controls is in line with the hypothesis of a generally reduced cerebrovascular compliance. In the patient groups, the peak flow traveled from MCA to SSS roughly in 60% the time it took to travel in age-matched controls. To our knowledge, this finding has not been reported previously.

Surprisingly, a significantly faster translation of the peak flow waveform was found in the MAPHSA-group compared with the (older) healthy age-matched control group. In addition, the PI ratio MCA/ICA for the MAPHSA group was larger than in the age-matched control, but without reaching statistical significance. These differences resemble the ones found in AD and MCI patients but in a less pronounced way. They could reflect an early manifestation of the vascular deterioration in a group of middle-aged individuals with parental history of sporadic AD.

In our study, we evaluated the PI ratio between two vessel segments as an additional parameter that reflects the ability of the vessels to dampen the pulse wave. We calculated the ratio of PI in the MCA over PI in the ICA to evaluate changes in pulsatility along the intracranial conduit arteries. MCA/ICA PI ratios showed a gradual increase from healthy aging over MCI to AD subjects with a significant difference between AD subjects and healthy age-matched individuals. This finding is in accordance with a reduced dampening of the pulse wave in AD and MCI patients. We also calculated the PI ratio SSS/ICA and the groups' trends are the same, with significant differences between the AD and age-matched controls (Supplementary Material).

Differences in blood pressure that may lead to altered pulsatility between the AD, MCI, and age-matched groups can be excluded in our study (Supplementary Material).

A relation between AD and the destructive impact of the pulse on the cerebral vasculature has been suggested.[11] Moreover, it has been proposed that insufficient dampening of the pulse wave leads to damage of the deep perforating arterioles.[41] These vessels are especially vulnerable to increased pulsatility as they cannot be sufficiently protected by prearteriolar sphincters due to the constant high demand of blood of the brain. Our results indicate that the pulse wave is least dampened in AD patients, potentially resulting in damage to the arterioles and subsequently the capillary bed. Accordingly, a higher degree of arteriolar kinking and looping has been reported in histopathological analyses of AD patients, indicating exposure to higher pulsatile stress.[42] Further, histopathologic changes that underline a vascular contribution to AD include the appearance of string vessels (collapsed and acellular membrane tubes), a reduction in capillary density, a rise in endothelial pinocytosis, and a decrease in mitochondrial content, which result in breakdown of the blood–brain barrier with leakage of blood-borne molecules.[43]

There are some limitations to our study. The sample size was limited to 26 subjects per group. Ideally, this number would have been larger. Consequently, sample size should be taken into account when interpreting the findings here. Ideally, we would have acquired a low venc and high venc PC VIPR acquisition to broaden the range of velocities in the analysis, but this acquisition would have taken 14 min and this amount of time was not clinically feasible in the study protocol. Although inherent errors exist in the calculation of flow rates and PI, namely spatial resolution variation due to the intrinsic averaging of MRI and the inherent noise, the same methodology is applied to each subject, and should result in group wise differences when comparing this calculation over large cohorts.

In summary, this study provides evidence regarding a significant vascular component to AD pathogenesis. New characteristics of the hemodynamic parameters of both arterial and venous vasculature as well as the transit time of the pulse wave are presented. The feasibility of hemodynamic analysis over a large vascular territory in the context of AD with 4D flow MRI within a 7 min acquisition is demonstrated. With the large volume coverage and high temporal and spatial resolution demonstrated here, 4D flow MRI enables angiographic and quantitative assessment, and therefore can provide biomarkers of vascular health that can contribute to increase understanding of the pathogenesis of AD and help in the treatment of AD patients.

Funding

The author(s) disclosed receipt of the following financial support for the research, authorship, and/or publication of this article: NIH (NIA grant P50-AG033514, NIHLBI R01HL072260, and NIGMS R25GM083252); Tilman Schubert is supported by a fellowship grant (Helmut-Hartweg-Fonds) from the Swiss Academy of Medical Sciences.

Acknowledgments

We gratefully acknowledge GE Healthcare for their assistance and support. The content is solely the responsibility of the authors and does not necessarily represent the official views of the NIH.

Declaration of conflicting interests

The author(s) declared no potential conflicts of interest with respect to the research, authorship, and/or publication of this article.

Authors' contributions

Leonardo A Rivera-Rivera: Study design, 4D flow MRI data reconstruction and post processing analysis; statistical analysis, interpreting results, editing of the manuscript and figures. Tilman Schubert: Study design, interpreting results, editing of the manuscript and figures. Patrick Turski: Clinical neuroradiologist, clinical input and selection of the regions of interest for flow analysis, components of study design, image quality review, editing of the manuscript and\ figures. Kevin M Johnson: Optimization of 4D flow MRI sequence designs and image reconstruction. Sara E Berman: assisted with methods section writing, specifically the subjects and clinical classification and cognitive assessment sections; editing of the manuscript. Howard A Rowley: Imaging protocols, design of non-flow imaging analysis, oversight of imaging acquisition, image quality insurance, maintaining of the imaging archives and assessment of brain morphology for comorbid diseases. Cynthia M Carlsson: Clinical supervising physician for medical data collection, interpreting the results and editing of the manuscript. Sterling C Johnson: Study design, data acquisition, interpreting results and editing of the manuscript. Oliver Wieben: 4D flow MRI sequence designs, study design, interpreting results, editing of the manuscript and figures.

Supplementary material

Supplementary material for this paper can be found at http://jcbfm.sagepub.com/content/by/supplemental-data

References

1. Querfurth HW and LaFerla FM. Alzheimer's disease. *N Engl J Med* 2010; 362: 329–344.
2. Neumann MA and Cohn R. Neuropathologic data in Alzheimer's disease. *Arch Neurol* 1983; 40: 830–831.
3. The Ronald and Nancy Reagan Research Institute of the Alzheimer's Association and the National Institute on Aging Working Group. Consensus report of the Working Group on: ''Molecular and Biochemical Markers of Alzheimer's Disease". *Neurobiol Aging* 1998; 19: 109–116.
4. Roher AE. Cardiovascular system participation in Alzheimer's disease pathogenesis. *J Intern Med* 2015; 277: 426–428.
5. Cullen KM, Kocsi Z and Stone J. Microvascular pathology in the aging human brain: Evidence that senile plaques are sites of microhaemorrhages. *Neurobiol Aging* 2006; 27: 1786–1796.
6. Kumar-Singh S, Pirici D, McGowan E, et al. Dense-core plaques in Tg2576 and PSAPP mouse models of Alzheimer's disease are centered on vessel walls. *Am J Pathol* 2005; 167: 527–543.
7. Fischer CE, Qian W, Schweizer TA, et al. Lewy bodies, vascular risk factors, and subcortical arteriosclerotic leukoencephalopathy, but not Alzheimer pathology, are associated with development of psychosis in Alzheimer's disease. *J Alzheimers Dis* 2015; 50: 283–295.
8. Kyrtsos CR and Baras JS. Modeling the role of the glymphatic pathway and cerebral blood vessel properties in Alzheimer's disease pathogenesis. *PLoS One* 2015; 10(10): e0139574.
9. Rivera-Rivera LA, Turski P, Johnson KM, et al. 4D flow MRI for intracranial hemodynamics assessment in Alzheimer's disease. *J Cerebr Blood Flow Metab*. Epub ahead of print 25 November 2015. DOI: 10.1177/0271678X15617171.
10. Liu G, Yao L, Liu J, et al. Cardiovascular disease contributes to Alzheimer's disease: Evidence from large-scale genome-wide association studies. *Neurobiol Aging* 2014; 35: 786–792.
11. Stone J, Johnstone DM, Mitrofanis J, et al. The mechanical cause of age-related dementia (Alzheimer's disease): the brain is destroyed by the pulse. *J Alzheimers Dis* 2015; 44: 355–373.
12. Jellinger KA. Alzheimer disease and cerebrovascular pathology: an update. *J Neural Transm* 2002; 109: 813–836.
13. Bateman GA, Levi CR, Schofield P, et al. The venous manifestations of pulse wave encephalopathy: windkessel dysfunction in normal aging and senile dementia. *Neuroradiology* 2008; 50: 491–497.
14. Bateman GA. Pulse wave encephalopathy: A spectrum hypothesis incorporating Alzheimer's disease, vascular dementia and normal pressure hydrocephalus. *Med Hypotheses* 2004; 62: 182–187.
15. Henry-Feugeas MC, Onen F and Claeys ES. Classifying late-onset dementia with MRI: Is arteriosclerotic brain degeneration the most common cause of Alzheimer's syndrome? *Clin Interv Aging* 2008; 3: 187–199.
16. Byrom FB. The pathogenesis of hypertensive encephalopathy and its relation to the malignant phase of hypertension; experimental evidence from the hypertensive rat. *Lancet* 1954; 267: 201–211.
17. Schubert T, Pansini M, Bieri O, et al. Attenuation of blood flow pulsatility along the Atlas slope: a physiologic property of the distal vertebral artery? *AJNR Am J Neuroradiol* 2015; 36: 562–567.
18. Schubert T, Santini F, Stalder AF, et al. Dampening of blood-flow pulsatility along the carotid siphon: does form follow function? *AJNR Am J Neuroradiol* 2011; 32: 1107–1112.
19. Zarrinkoob L, Ambarki K, Wahlin A, et al. Aging alters the dampening of pulsatile blood flow in cerebral arteries. *J Cereb Blood Flow Metab* 2016. Epub ahead of print 28 January 2016. DOI: 10.1177/0271678X16629486.
20. Morris AWJ, Carare RO, Schreiber S, et al. The cerebrovascular basement membrane: role in the clearance of

β-amyloid and cerebral amyloid angiopathy. *Front Aging Neurosci* 2014; 6: 251.
21. Carare RO, Hawkes CA, Jeffrey M, et al. Review: cerebral amyloid angiopathy, prion angiopathy, CADASIL and the spectrum of protein elimination failure angiopathies (PEFA) in neurodegenerative disease with a focus on therapy. *Neuropathol Appl Neurobiol* 2013; 39: 593–611.
22. Weller RO, Subash M, Preston SD, et al. Perivascular drainage of amyloid-beta peptides from the brain and its failure in cerebral amyloid angiopathy and Alzheimer's disease. *Brain Pathol* 2008; 18: 253–266.
23. Gupta A and Iadecola C. Impaired Ab clearance: a potential link between atherosclerosis and Alzheimer's disease. *Front Aging Neurosci* 2015; 7: 115. DOI: 10.3389/fnagi.2015.00115.
24. Hawkes CA, Jayakody N, Johnston DA, et al. Failure of perivascular drainage of b-amyloid in cerebral amyloid angiopathy. *Brain Pathol* 2014; 24: 396–403.
25. Roher AE, Garami Z, Tyas SL, et al. Transcranial Doppler ultrasound blood flow velocity and pulsatility index as systemic indicators for Alzheimer's disease. *Alzheimers Dement* 2011; 7: 445–455.
26. Markl M, Frydrychowicz A, Kozerke S, et al. 4D flow MRI. *J Magn Reson Imag* 2012; 36: 1015–1036.
27. Peters DC, Korosec FR, Grist TM, et al. Undersampled projection reconstruction applied to MR angiography. *Magn Reson Med* 2000; 43: 91–101.
28. Frydrychowicz A, Wieben O, Niespodzany E, et al. Quantification of thoracic blood flow using volumetric magnetic resonance imaging with radial velocity encoding: in vivo validation. *Invest Radiol* 2013; 48: 819–825.
29. Chang W, Landgraf B, Johnson KM, et al. Velocity measurements in the middle cerebral arteries of healthy volunteers using 3D-radial PC HYPRFlow: comparison with transcranial Doppler sonography and 2D phase-contrast MR imaging. *AJNR Am J Neuroradiol* 2011; 32: 54–59.
30. Wahlin A, Ambarki K, Birgander R, et al. Measuring pulsatile flow in cerebral arteries using 4D phase-contrast MR imaging. *Am J Neuroradiol* 2013; 34: 1740–1745.
31. Sager MA, Hermann B and La Rue A. Middle-aged children of persons with Alzheimer's disease: APOE genotypes and cognitive function in the Wisconsin Registry for Alzheimer's Prevention. *J Geriatr Psychiatry Neurol* 2005; 18: 245–249.
32. McKhann G, Drachman D, Folstein M, et al. Clinical diagnosis of Alzheimer's disease: report of the NINCDS-ADRDA Work Group under the auspices of Department of Health and Human Services Task Force on Alzheimer's Disease. *Neurology* 1984; 34: 939–944.
33. Gu T, Korosec FR, Block WF, et al. PC VIPR: a high-speed 3D phase-contrast method for flow quantification and high resolution angiography. *AJNR Am J Neuroradiology* 2005; 26: 743–749.
34. Johnson K, Lum D, Turski P, et al. Improved 3D phase contrast MRI with off-resonance corrected dual echo VIPR. *Magn Reson Med* 2008; 60: 1329–1336.
35. Liu J, Redmond MJ, Brodsky EK, et al. Generation and visualization of four dimensional MR angiography data using an undersampled 3-D projection trajectory. *IEEE Trans Med Imaging* 2006; 25: 148–157.
36. Schrauben E, Wåhlin A, Ambarki K, et al. Fast 4D flow MRI intracranial segmentation and quantification in tortuous arteries. *J Magn Reson Imaging* 2015; 42: 1458–1464.
37. O'Rourke MF and Hashimoto J. Mechanical factors in arterial aging: a clinical perspective. *J Am Coll Cardiol* 2007; 50: 1–13.
38. Stoquart-ElSankari S, Baledent O, Gondry-Jouet C, et al. Aging effects on cerebral blood flow and cerebrospinal fluid flows. *J Cereb Blood Flow Metab* 2007; 27: 1563–1572.
39. Kim J, Thacker NA, Bromiley PA, et al. Prediction of the jugular venous waveform using a model of CSF dynamics. *AJNR Am J Neuroradiol* 2007; 28: 983–989.
40. Bateman GA. Pulse-wave encephalopathy: a comparative study of the hydrodynamics of leukoaraiosis and normal-pressure hydrocephalus. *Neuroradiology* 2002; 44: 740–748.
41. Henry-Feugeas MC, Roy C, Baron G, et al. Leukoaraiosis and pulse-wave encephalopathy: observations with phase-contrast MRI in mild cognitive impairment. *J Neuroradiol* 2009; 36: 212–218.
42. Fischer VW, Siddiqi A and Yusufaly Y. Altered angioarchitecture in selected areas of brains with Alzheimer's disease. *Acta Neuropathol* 1990; 79: 672–679.
43. Zlokovic BV. Neurovascular pathways to neurodegeneration in Alzheimer's disease and other disorders. *Nat Rev* 2011; 12: 723–738.